Light-Controlled Large-Scale Wirelessly Reconfigurable Microstrip Reflectarrays

Si Yu Miao, *Student Member, IEEE*, and Feng Han Lin, *Senior Member, IEEE*

***Abstract*— In this article, the concept and design of light-controlled large-scale wirelessly reconfigurable microstrip reflectarrays are proposed. Unlike conventional electrically reconfigurable microstrip reflectarray antennas (RAs) that control the aperture phase distribution by conducting wires for transmitting control signals, the proposed method utilizes light to control the ON- and OFF-state of the integrated positive-intrinsic-negative (p-i-n) diodes wirelessly and binaurally through light-sensitive resistance of photodiodes (PDs). The concept is validated by simulation first, where a 1 bit 32 × 32 wirelessly reconfigurable microstrip RA is designed at 10 GHz with a beam-steering range of ±60° for sidelobe levels <−10 dB, marking a record of 1024 elements with a tri-layer configuration. Experimentally, the light-control scheme is further validated by a smaller porotype of 256 elements, where a light-controlled beam steering from 30° to 45° is demonstrated. Compared with conventional wired reconfigurable microstrip RAs, the proposed method resolves the wire-routing complexity on the RA and offers a new possibility for further improving the maximum directivity, upper operating frequency, and the number of independently controllable polarizations of reconfigurable microstrip reflectarrays, paving the way for developing very-large reconfigurable intelligent surfaces (VRIS). Also, the proposed concept provides a new infrastructure for information exchange between light and microwaves.**

***Index Terms*— Beam steering, light control, metamaterials, metasurface, reconfigurable antenna, reconfigurable intelligent surface, reconfigurable reflectarray.**

I. Introduction

THE next generation of the wireless network (6G) calls for economic antenna solutions to challenging problems concerning continuous space coverage, hybrid near-/far-field beamforming, multi-user positioning/sensing, and holographic multiple-in-multiple-out (MIMO), where low-cost high-gain beam-steerable antennas are highly desired [1], [2]. Compared with conventional microstrip phased arrays, reconfigurable microstrip reflectarray antennas (RAs) are advantageous in low loss and low cost due to simpler feeding networks and fewer transmit/receive (T/R) modules [3]. However, the size scalability, the operating frequency, and the number of polarizations of conventional reconfigurable microstrip RAs are limited by the most widely adopted wire-control architecture, hence further hindering the generation of multi-polarization multi-beams of high gain in millimeter wave bands. By wire-control, it means that conducting wires are used to transmit control signals to tunable components or materials for reconfiguring the distribution of aperture fields.

Three methods are typically used for designing reconfigurable microstrip RAs, where the electrical method is mostly adopted [4], [5], [6], [7], [8], [9], [10], [11], [12], [13], [14], [15], [16], [17], [18], [19], [20], [21], [22], compared to the mechanical method [23], [24], [25], [26] and optical method recently proposed [27], [28], [29]. For the electrical method, the key is to design the reconfigurable elements with tunable components or tunable materials, such as the positive-intrinsic-negative (p-i-n) diode switches [4], [5], [6], [7], [8], varactors [9], [10], [11], microelectromechanical (MEMS) switches [12], [13], [14], liquid crystals (LCs) [15], [16], [17], [18], phase-changing materials [19], ferroelectric materials [20], and graphene [21], [22]. The listed components or materials are further used in three different ways, as detailed in the following.

As binary switches, p-i-n diodes are often loaded between a delay line and a microstrip patch antenna for different reflection phases switched through the diodes at a speed of nanoseconds [4], [7]. The p-i-n diode switches can be replaced by microelectromechanical (MEMS) switches for lower insertion loss, at the cost of longer switching time (typically a few microseconds), higher driving voltage (typically tens of volts for static-electric actuation for example), and higher cost of manufacturing due to incompatible fabrication process [30].

As lumped reactive loadings, varactor diodes are often used instead as tunable capacitors loaded on an antenna for continuous adjustment of its reflection phase by tuning the biasing voltage of the diodes, at the cost of higher biasing voltage (typically tens of volts) and lower tuning speed at a microsecond level [9], [10], [11].

As distributed reactive loadings, tunable materials are often used. For example, uniaxial LCs can be used as substrate or superstrate of an antenna, whose reflection phase changes with the varying effective permittivity of the loaded LC, subject to the biasing electric field applied onto the LC, providing a tuning speed in a level of milliseconds [15], [16], [17], [18]. Similarly, phase-changing materials, such

Manuscript received 3 May 2022; revised 26 October 2022; accepted 3 December 2022. Date of publication 23 December 2022; date of current version 3 February 2023. This work was supported in part by the National Key Research and Development Project of China under Grant 2022YFB2902800, in part by the National Natural Science Foundation of China (NSFC) under Grant 62101330, in part by the Lingang Laboratory under Grant LG-QS-202202-05, and in part by the Shanghai Pujiang Program under Grant 20PJ1411400. *(Corresponding author: Feng Han Lin.)*

The authors are with the School of Information Science and Technology, ShanghaiTech University, Shanghai 201210, China (e-mail: miaosy@shanghaitech.edu.cn; linfh@shanghaitech.edu.cn).

Color versions of one or more figures in this article are available at https://doi.org/10.1109/TAP.2022.3230551.

Digital Object Identifier 10.1109/TAP.2022.3230551

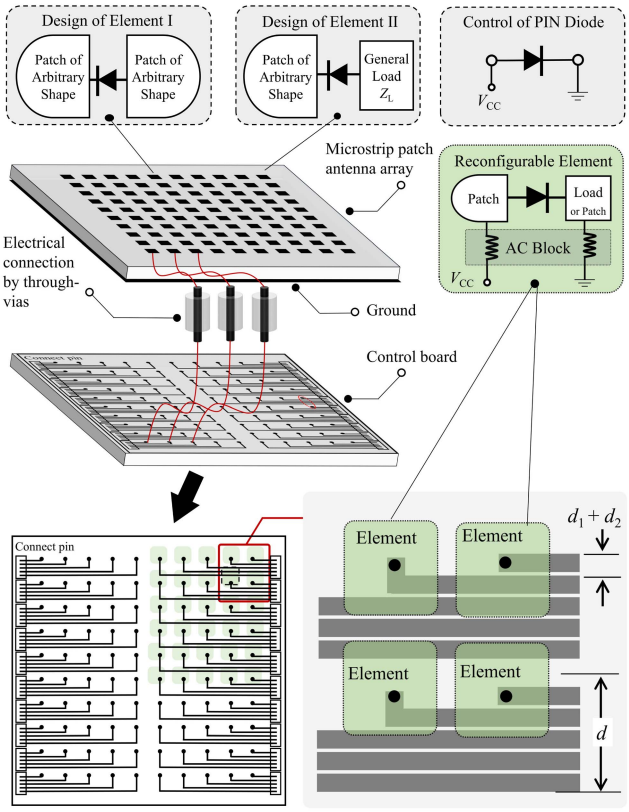

Fig. 1. Conceptual illustration of typical element configuration of reconfigurable microstrip reflectarray, circuitry of p-i-n diode, and the routing of controlling wires behind a generic 10×10 reconfigurable RA.

as vanadium diode (VO_2), can be loaded on a metasurface antenna whose operating frequency changes with the states of the VO_2, subject to the applied biasing E-field [19]. The tuning speed of VO_2 is at a nanosecond level [31]. Also, ferroelectric materials such as barium strontium titanate (BST) are used for beam steerable reflectarrays by changing the constitutive parameters with biasing magnetic field [20]. Graphene is used in beamscanning reflectarrays by tuning the conductivity with biasing E-field [21], [22].

Among the above, p-i-n diodes are the most commonly used in reconfigurable microstrip RAs for their low power consumption, fast switching speed, and ease of integration and biasing [30]. Fig. 1 shows a generic example of an $N \times N$ reconfigurable microstrip RA using p-i-n diodes ($N = 10$ for example). Overall, the RA includes a microstrip antenna array and a control board behind the ground, which are interconnected by through-vias [4], [5]. The insets of Fig. 1 show two typical methods for designing a reconfigurable antenna element. In the design of element I, a p-i-n diode connects two separable parts of the microstrip patch antenna for a reconfigured shape of the microstrip patch resonator. In the design of element II, a p-i-n diode connects the microstrip patch antenna to a general load impedance Z_L that can be realized by an open-circuited transmission line for example. Detailed examples of implementing the two methods can be found in [6] and [4], respectively. Nevertheless, for both methods, the biasing voltage of each p-i-n diode is controlled individually by a conducting wire on the control board. As a result, the total number of wires (and the occupied area by which) increases along with the number of diodes. Furthermore, the number of diodes mainly depends on the number of tunable array elements, the number of polarizations, and the phase bits needed. Therefore, the use of wires-control p-i-n diodes can cause three limitations for reconfigurable microstrip reflectarrays, including the highest directivity, the upper operating frequency, and the number of independently controllable polarizations.

Fig. 1 illustrates the cause of the three limitations graphically in the bottom insets at the bottom, where the control board and an enlarged part of it are shown in more detail. As can be seen from the bottom left of the figure, the wires connected to the arrays are oriented toward the board edges for further connection to external programming devices such as a field programmable gate array (FPGA) [32], [33]. At the bottom right, the shadows show the outlines of the patch antennas on the opposite side for reference. Observing either half of one row of the RA does not lose generality. It can be derived that

$$n \leq \frac{d}{(d_1 + d_2)} \tag{1}$$

where n is the number of control wires between two neighboring elements, d is the element spacing, d_1 is the minimum wire width, and d_2 is the minimum wire spacing. As can be seen, the maximum number of wires allowed between two rows appears bounded by the antenna spacing and the fabrication limit of printed traces when printed circuit board (PCB) technology is used, though the number of rows is not limited. Caused of this bound, the aforementioned three limitations are further explained in the following.

First, the directivity of the reconfigurable microstrip RAs is limited. Generally, higher directivity requires a larger array of a greater number of elements and controlling wires, thereby requiring a larger element spacing d to accommodate the growing number of wires. To simplify the understanding by an extreme case, we consider an array of an infinite number of microstrip elements that need an infinite number of diodes and controlling wires. Submitting $n = \infty$ into (1) leads to two conclusions. First, for a given element spacing d, $d_1 + d_2$ has to be infinitely small, which is apparently impossible. Second, for a given fabrication limit or the smallest $(d_1 + d_2)$, the element spacing d has to be infinitely large, which causes grating lobes upon scanning according to the well-known theory of antenna arrays. To resolve the dilemma, the large-scale RAs can be divided into subarrays [32], [33]. For example, a 1600-element reconfigurable RA is divided into five subarrays in [32] at the cost of a relatively slower beam steering because the adopted shift registers need time for data writing [33]. Without shift registers, a 10 240-element reconfigurable RA is divided into 40 subarrays in [33] and controlled by approximately 160 FPGAs, at the cost of more complex biasing networks and interconnections between the antenna system and digital control systems, where the delay and synchronization of the digital signals become the main challenge.

In addition to directivity, the operating frequency is also limited. As the operating frequency increases, the element spacing d tends to decrease geometrically (assuming electrically unchanged), between which fewer wires can be placed. For example, assume that a RA operates at a frequency f with a given element spacing d in wavelength. When the operating frequency increases to m times of f, the element spacing becomes $d' = d/m$. Again, consider an extreme case with m approaching infinity, so d' approaches 0, meaning that all the antenna elements have to be either overlapped or infinitely small. In addition, the number of wires n between two rows is also approaching zero, meaning no wires can be placed at an infinitely high frequency. This is an extreme case for understanding the limit. In practice, the highest operating frequency of the reconfigurable RA can be determined once the fabrication limit and the number of antenna elements are given.

Last but not the least, the number of controllable polarizations is limited. In wireless communication systems, an additional polarization implies an additional RF chain for enhanced communication capacity, which has led to the development of dual-polarized antennas. Herein, to include a second polarization for dual-polarized reconfigurable RAs, the number of p-i-n diodes and controlling wires should be at least doubled for independent control of each polarization, which again causes the aforementioned issue of wire placement.

The above challenges may be released by using more precise microelectronic manufacturing, at the cost of higher fabrication cost, smaller driving current, limited manufacturing size, and stronger crosstalk between control wires running high-speed digital signals. Alternatively, the wires may be placed in different layers. The disadvantages include higher manufacturing cost and fabrication difficulty due to the multilayer binding process, blind holes, and buried holes, which may be acceptable for PCB fabrication but difficult to implement on substrates like silicon wafers, glasses, and flexible films.

Recently, optically controlled metasurfaces have been proposed for manipulating electromagnetic waves in a wireless manner without complex wired biasing networks [27], [28], [29]. The pioneering work of a light-biased metamaterial structure has demonstrated a tunable reflection phase in [27], where the varactors loaded on split-ring resonators are biased by voltages generated by photo cells (PCs) that convert light into electric currents as solar cells do. In [29], multiple PCs are connected in series to generate light-controlled voltage for biasing multiple varactors loaded on a reflective metasurface. Therein, 36 reconfigurable elements are demonstrated with an element spacing of 0.87 wavelengths at the center frequency. The large element spacing is not suitable for wide-angle beam-steering antenna arrays (grating lobe issue) because a large area is needed for the PCs to generate high enough biasing voltage.

In this article, the concept and design of light-controlled large-scale wirelessly reconfigurable microstrip RAs are proposed. Instead of using conducting wires or light-powered high-voltage varactors, the combination of low-voltage p-i-n -diode switches and light-sensitive photodiodes (PDs) is proposed. The resistance of the PD is reconfigured wirelessly by binary light illumination, and so do the ON and OFF state of the p-i-n diode and the associated reflection phase of each antenna element, fundamentally breaking the limitations of directivity, operating frequency, and number of polarizations caused by wired control.

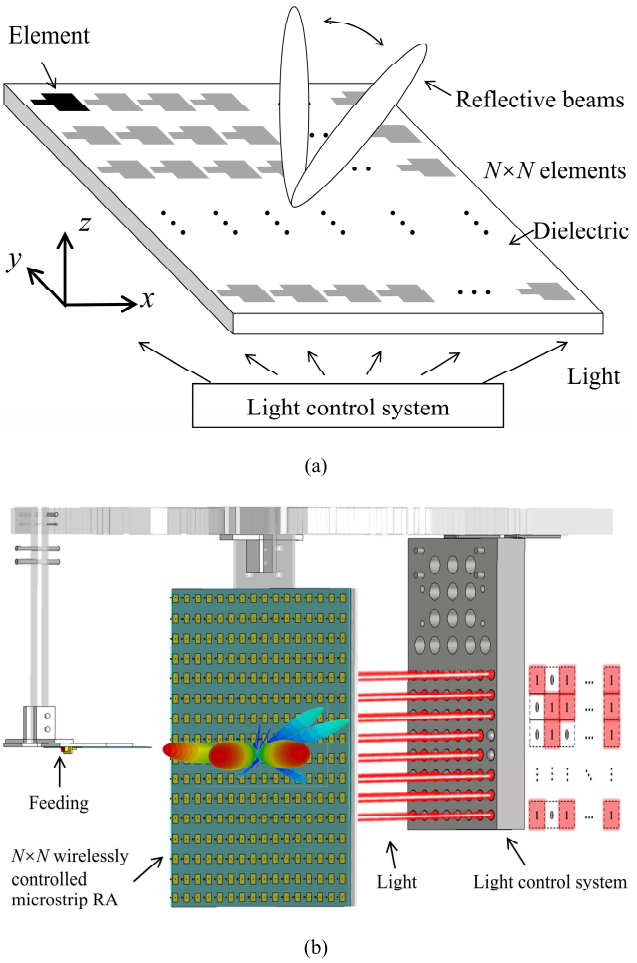

Fig. 2. Proposed light-controlled reconfigurable reflectarray system. (a) Concept illustration and system architecture. (b) Proof-of-concept design of the 1-bit light-controlled reconfigurable reflectarray system fed by a Vivaldi antenna.

Section II presents the architecture of the proposed wirelessly reconfigurable microstrip RA, including the overall configuration and the basic operating principle. Section III presents the design and simulation of a 1024-element wirelessly reconfigurable microstrip RA for proof of concept. Section IV presents the experimental results of a 256-element design for verifying the light-control scheme, followed by the conclusion in Section V. All simulations are carried out with the CST Microwave Studio Suite 2022 [34].

II. System Architecture: Wirelessly-Controlled Reconfigurable Reflectarray

Fig. 2(a) illustrates the proposed concept of the wirelessly controlled microstrip RA. As can be seen, the wirelessly reconfigurable RA consists of an array of $N \times N$ 1 bit reconfigurable microstrip patch antenna elements controlled by a light control system. Fig. 2(b) shows a more detailed

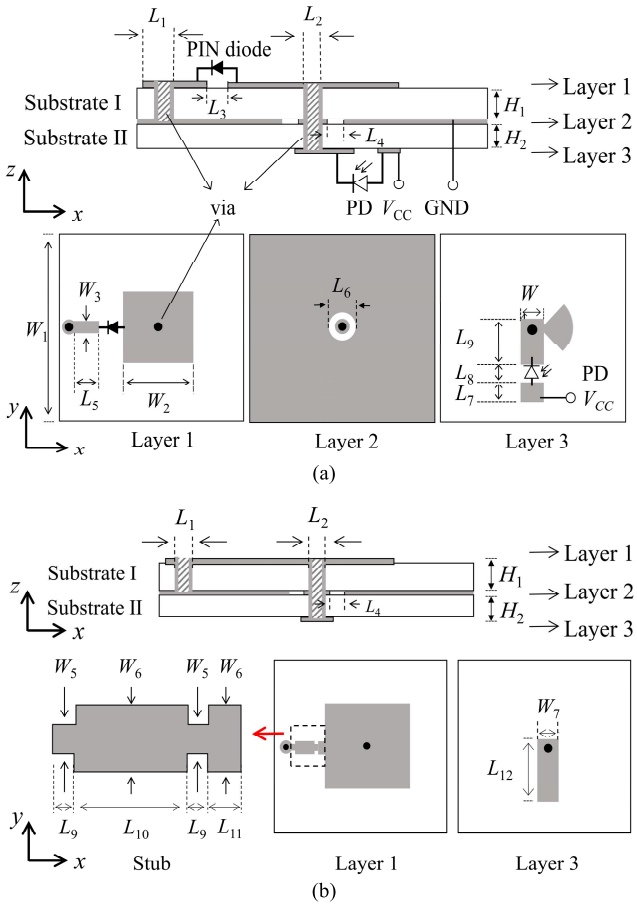

Fig. 3. Configurations of (a) active element controlled by light beams and (b) passive element controlled by manual cutting.

implementation with $N = 16$ for example. As can be seen, the controlling wires in conventional wire-controlled reconfigurable microstrip RAs are replaced by light beams, each of which controls one reconfigurable element individually in a binary and remote manner by switching the light ON and OFF with a coding matrix.

In the subsequent sections, two microstrip RAs are designed at 10 GHz for different purposes. The first one of 1024 elements is designed to verify the concept and advantages by numerical simulation. The second one of 256 elements is designed on an affordably smaller scale and measured to verify the light-control scheme.

III. Light-Controlled Reconfigurable Reflectarray

A. Modeling and Design of 1 Bit Reconfigurable Element

Two types of antenna elements are designed. Fig. 3(a) and (b) shows the proposed light-controlled reconfigurable element and the manually-controlled reconfigurable element, referred to as an active element and passive element, respectively, in the subsequent discussion. Detailed dimensions are summarized in Table I. In the simulation design of the 1024-element RA, all elements are active elements. In the 256-element RA designed and measured, some of the active elements are replaced by passive elements for low-cost experimental verification.

TABLE I
Dimensions of Active and Passive Elements (Unit: mm)

Parameter	L_1	L_2	L_3	L_4	L_5	L_6	L_7	L_8
Value	0.9	0.6	0.5	0.5	2.45	1.2	3	0.7
Parameter	L_9	L_{10}	L_{11}	L_{12}	W_1	W_2	W_3	W_4
Value	1	1.32	0.5	4.7	15	7.1	0.9	1
Parameter	W_5	W_6	W_7	H_1	H_2			
Value	0.5	1	1.5	1.524	1			

As can be seen from Fig. 3(a), the active element consists of three metallic layers with two layers of substrates in between. The dielectric constants of substrate I and substrate II are 3.55 (loss tangent 0.004) and 4.4 (loss tangent 0.025), respectively. The microstrip line on layer 3 is rotated by 90° with respect to the z-axis for better illustration in a cross section view. On top layer 1, a square patch and a grounded microstrip line are connected by a p-i-n diode. For biasing the p-i-n diode, the direct-current (dc) voltage V_{cc} is supplied by a through-ground via from the bottom layer 3, which is further controlled by the light-sensitive resistance of a PD. As a result, the ON and OFF state of the p-i-n diode, hence the reflection phase of each antenna element, can be reconfigured by switching ON and OFF the light projected on each PD. The resistance of the PD switches between tens of ohms (Ω) in a bright mode (with light) and mega ohms (MΩ) in a dark mode (without light). The part numbers of the p-i-n diode and PD are MADP-000402-12530P and PTSMD021, respectively. The active element operates in State 1 when the p-i-n diode and PD are both in ON states (bright mode), otherwise in State 0 for OFF states (dark mode).

Two measures are taken to minimize the impact of the circuitry over layer 3 on the radiation performance of the RA. First, the biasing via is located at the null of the E-field of the TM_{10} mode of the patch antenna for minimized high-frequency currents over the via. Second, the via is virtually grounded by a virtually short-circuited microstrip stub, which prevents the high-frequency currents from going into the dc circuits [35].

The passive element in Fig. 3(b) is designed in three steps. First, both the p-i-n diode and the PD are removed. Second, the passive element is slightly optimized to mimic the loading effects of the p-i-n diode, for achieving the same reflection coefficients as those of the active element in both the bright and dark modes. Third, to mimic the active element in dark mode, part of the passive element is designed for being cut manually, which in Fig. 3(b) is the narrower part with a length of L_9 and a width of W_5. In this way, the passive element can be reconfigured manually between two states.

The operating principle of light-controlled p-i-n switches in active elements is further explained. For the p-i-n diode,

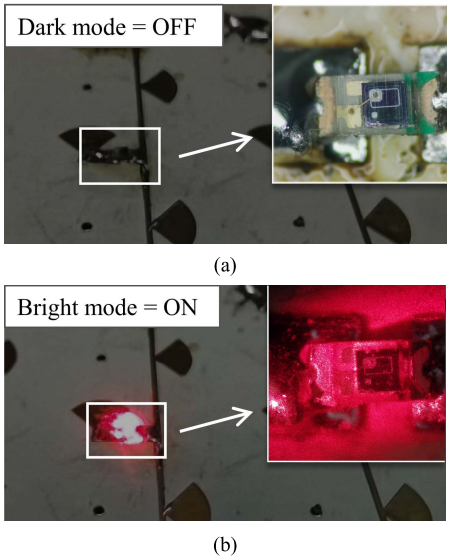

Fig. 4. Illustrations of the PD under two different conditions of light illumination. (a) Without light. (b) With light.

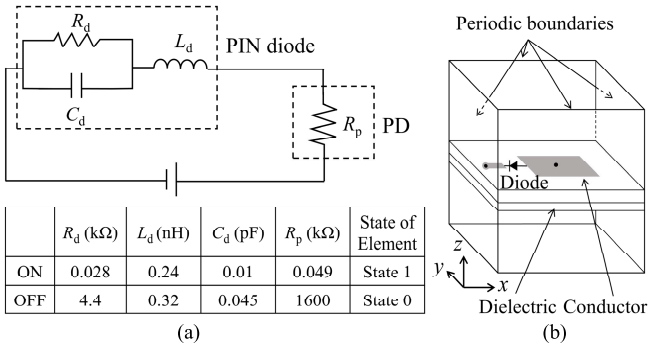

	R_d (kΩ)	L_d (nH)	C_d (pF)	R_p (kΩ)	State of Element
ON	0.028	0.24	0.01	0.049	State 1
OFF	4.4	0.32	0.045	1600	State 0

Fig. 5. Simulation model of the active element, including (a) equivalent circuit diagram of the p-i-n diode and the photodiode and (b) boundary setup for extracting the reflection phase of the active element.

the ON and OFF states are associated with a forward biasing voltage of 0.8 and 0 V, respectively. For the PD, the ON and OFF states denote the conditions with and without light illumination, as illustrated in Fig. 4(a) and (b), respectively, where a laser is used to control the resistance of the PD. The dark resistance of the PD (denoted by R_p) is measured with 1.6 MΩ approximately, which limits the maximum current through the circuit to a microampere-level for the OFF state of the p-i-n diode. On the contrary, the measured bright resistance decreases to 49 Ω, allowing for a current of a milliampere-level for the ON state of the p-i-n diode. As a result, the states of the p-i-n diode can be controlled by switching ON and OFF the light that illuminates the PD. In this way, the p-i-n diode switches ON and OFF the loading of the delay line to the patch antenna element for reconfigured reflection phase.

The geometric dimensions of the elements are designed with simulation, where the p-i-n diode and the PD are modeled by equivalent circuits as suggested in the datasheet [36], [37]. The detailed circuit diagrams of the modeling are shown in Fig. 5(a). As can be seen, the p-i-n diode is modeled as an

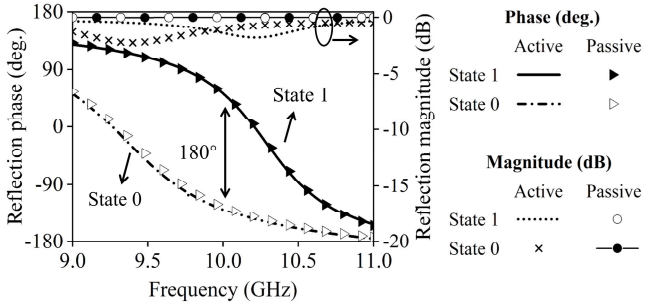

Fig. 6. Simulated reflection coefficients of the passive and active elements at different operating states (State 1 for light ON and State 0 for light OFF).

inductor of inductance L_d in series with a resistor of resistance R_d, where the latter is further shunted with a capacitor of an effective junction capacitance C_d [36]. The PD is modeled as a resistor of resistance R_p, which is designed not to affect the antenna performance. However, since the values of L_d, R_d, C_d, and R_p are not available, they are measured at 10 GHz by using an in-house developed transmission-line method with curve fitting. The measured values are tabulated in Fig. 5(a).

With the above circuit models of the two diodes included, Fig. 5(b) shows the setup of field-circuit co-simulation in CST Microwave Studio for achieving the reflection coefficient of the designed antenna element in different states [30]. Specifically, periodic boundary conditions are set at four sides with an x-polarized normal incidence toward the $-z$-direction. The periodicity is 0.5λ, where $\lambda = 30$ mm is the wavelength at 10 GHz. Two Floquet ports are defined on the top and bottom for calculating the scattering matrices at different frequencies.

Fig. 6 shows the simulated reflection coefficients in both magnitude and phase. As can be seen, the active and passive elements exhibit nearly the same reflection phases at 10 GHz with up to a 1 dB difference in magnitude. The effects of the 1 dB insertion loss on the radiation patterns of the array are investigated in simulation, showing no effect on the main-lobe directions, though 0.3 dB is worse than the sidelobe levels (not shown for brevity). Therefore, the active and passive elements can be swapped in the array design without affecting the effectiveness of validation. To be more specific, the insertion losses are approximately −1.4 dB for State 0 (dark mode) and −1 dB for State 1 (bright mode) for the active element. The phase difference between the two states is 180° at 10 GHz as desired. It is worth noting that the measured values of the p-i-n diode and the PD have already been considered in the simulation.

Fig. 7(a) shows the effects of different circuit models of the p-i-n diode (namely using R_d, L_d, and C_d only) on the reflection phase of the active element, useful for simplifying the simulation of a very-large-scale RA. Reference is made to the model with R_d, L_d, and C_d. For ease of comparison, Fig. 7(b) shows the phase difference between two states against different types of modeling. As can be seen in the band of observation, modeling the p-i-n diode by only R_d leads to a reflection phase and magnitude similar to the reference in both states. In light of the binary phase conversion

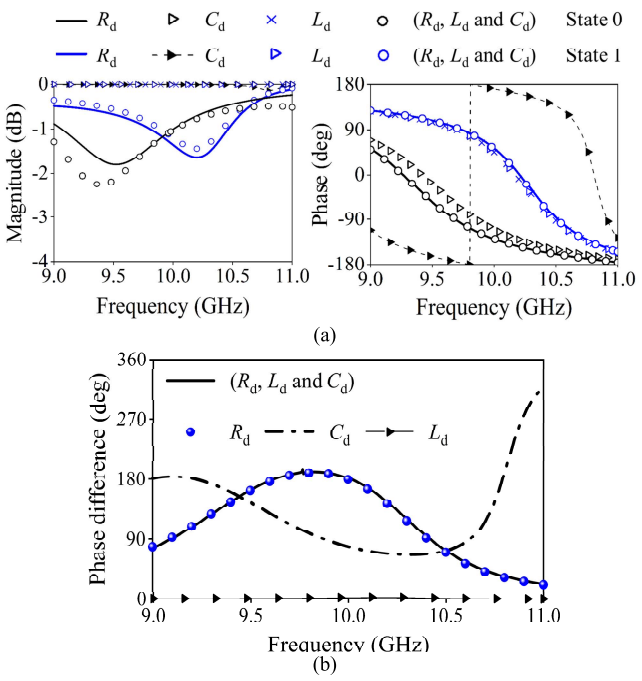

Fig. 7. Effects of different circuit models of the p-i-n diode on the reflection phase of the active element. (a) Magnitude and phase of the simulated reflection coefficients. (b) Phase difference between two states of the active element with different models of the p-i-n diode.

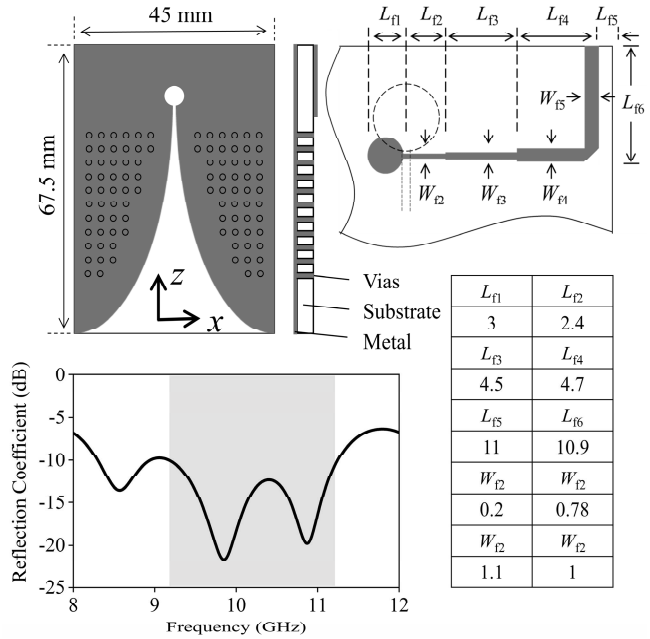

L_{f1}	L_{f2}
3	2.4
L_{f3}	L_{f4}
4.5	4.7
L_{f5}	L_{f6}
11	10.9
W_{f2}	W_{f2}
0.2	0.78
W_{f2}	W_{f2}
1.1	1

Fig. 8. Vivaldi antenna as feeding antenna: geometry, dimensions, and $|S_{11}|$.

for 1 bit wirelessly reconfigurable RA, the p-i-n diode can be reasonably modeled as an R_d in a very large full-array simulation for reduced computation cost.

B. Source Antenna

A Vivaldi antenna is designed to feed the RA due to its lower weight than horns, which facilitates the measurement. Fig. 8 shows the details of the Vivaldi antenna, including its

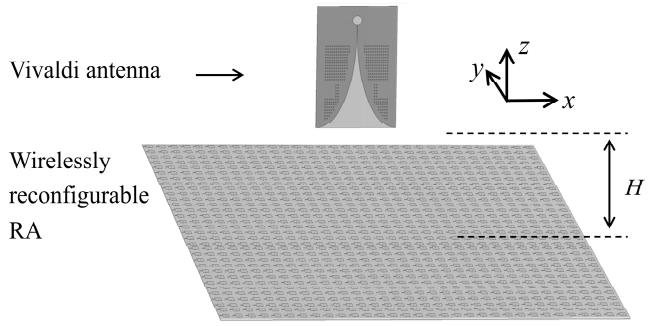

Fig. 9. Overall configuration and coordinate system of the proposed 1-bit wirelessly reconfigurable RA with 1024 elements, fed by a Vivaldi antenna.

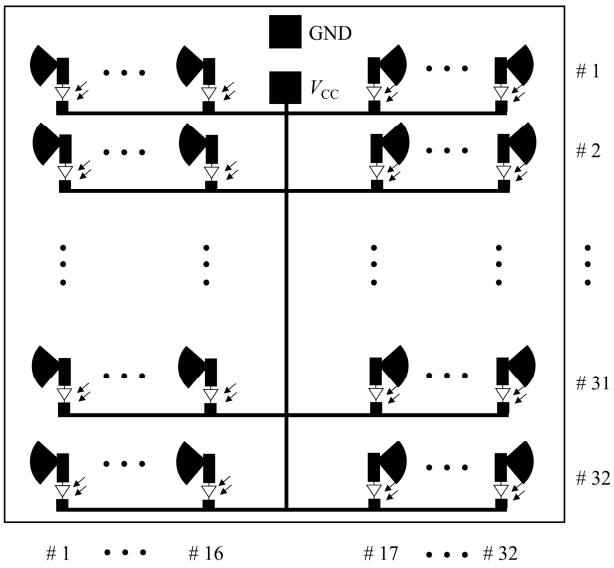

Fig. 10. DC-bias network of the wirelessly reconfigurable RA. A single trace connects all the PDs for voltage supply without complex wire routing.

geometry, feeding network, detailed dimensions, and reflection coefficients. The thickness, dielectric constant, and loss tangent of the substrate are 0.508 mm, 3.55, and 0.0027, respectively. The metallic vias improve the mechanical strength. The multi-section impedance transformers match the antenna to 50 Ω. with a 10 dB impedance bandwidth of 9.2–11.3 GHz and $|S_{11}| < -18$ dB at 10 GHz.

C. Simulation of the Proposed 32 × 32 Reflectarray

The active element designed earlier is arranged in an $N \times N$ array, where N can be an arbitrary integer. With $N = 32$, Fig. 9 shows the configuration of the 1024-element wirelessly reconfigurable RA, center fed by the Vivaldi antenna of normal incidence. Here, $N = 32$ is used for proof of concept, though it can be much larger or smaller, giving rise to an overall size of 480 × 480 mm. The distance is $H = 215$ mm between the center of the RA and that of the opening flare of the Vivaldi antenna for an illumination taper of −10 dB at the edge of the RA.

Fig. 10 shows the biasing network on the bottom layer of the wirelessly reconfigurable RA. The two square pads located at

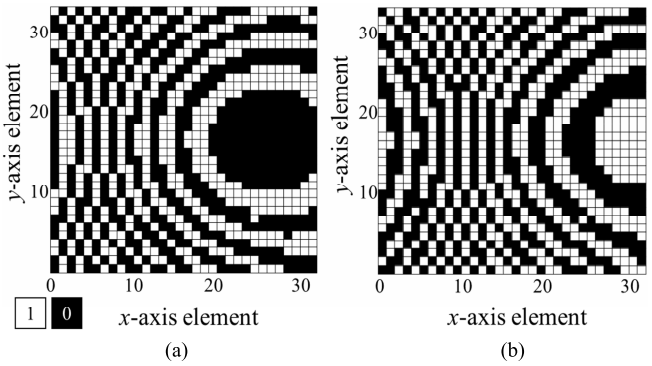

Fig. 11. Illustration of the binary states of p-i-n diodes for pointing two beams at (a) $\theta = 30°$. (b) $\theta = 45°$. White grids for elements in State 1 and black grids for elements in State 0.

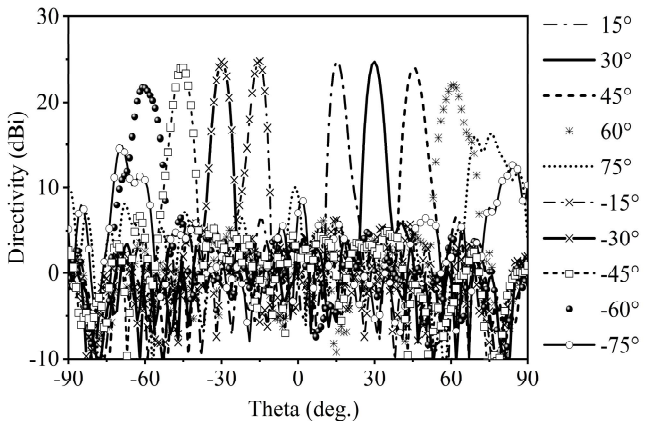

Fig. 12. Simulated E-plane radiation pattern at 10 GHz for the 1024-element wirelessly reconfigurable RA. The cross-polarization level is below −40 dB.

the top of the figure are dedicated to battery connection. As can be seen, only a single trace shunts all the elements for biasing all the PDs at once, without other additional wires, as compared to the conventional wire-controlled reconfigurable RA in Fig. 1. Therefore, the total number of elements is no longer limited by the area between two elements for wire placement. In fact, the saved spacing (by removing the controlling wires) also allows for a wider biasing trace for running higher driving current for high-power devices, paving the way for the development of advanced metasurface devices such as amplifying metasurfaces, mixing metasurfaces, computational metasurfaces, and neural-network metasurfaces.

For achieving beamsteering, the states of the elements are determined by the phase difference between the incident and reflected fields [38]. For example, Fig. 11 shows the binary phase difference $\Phi\ (x, y)$ for achieving maximum radiation at $\theta = 30°$ and $\theta = 45°$ (both with $\varphi = 0°$), respectively. The binary phase differences are achieved by setting $\Phi\ (x, y) < 0°$ as black grids, otherwise white grids. Using the elements to compensate for the phase differences by setting elements in the white grids as State 1 (light mode), otherwise State 0 (dark mode). By switching the states of the p-i-n diodes and PDs from the map indicated in Fig. 11(a) to that in Fig. 11(b), the beam is redirected from $\theta = 30°$ to $\theta = 45°$.

TABLE II
COMPARISON OF KEY FEATURES OF RECONFIGURABLE METASURFACES

Ref.	No. of wires on RA	No. of tunable elements	No. of dielectric layers	Tuning methods	Element spacing
[7]	196	196	3	PIN diode	0.4 λ
[39]	256	256	2	PIN diode	0.475 λ
[8]	256	256	4	PIN diode	0.44 λ
[6]	144	144	2	PIN diode	0.55 λ
[40]	100	100	2	PIN diode	0.5 λ
[29]	0	36	2	Varactor and PC	0.87 λ
This work	0	1024	2	PIN diode and PD	0.5 λ

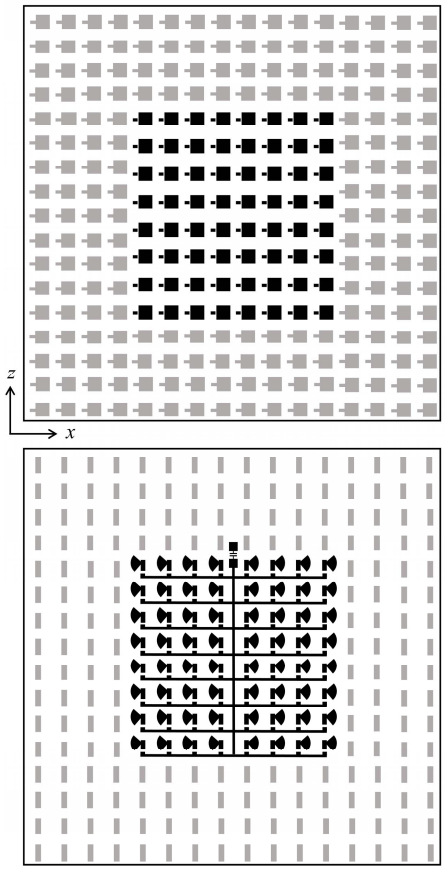

Fig. 13. Top and bottom views of the 16 × 16 wirelessly reconfigurable microstrip RA for experimental verification of the light-control scheme.

By simulation, the scanning performance of the 1024-element wirelessly reconfigurable RA is evaluated at five designed angles. Fig. 12 shows the simulated radiation patterns in the E-plane ($\varphi = 0°$). As can be seen, the main lobe is directed accurately to $\theta = 15°$, 30°, 45°, 60°, and 75°, respectively. However, the main beam splits upon scanning

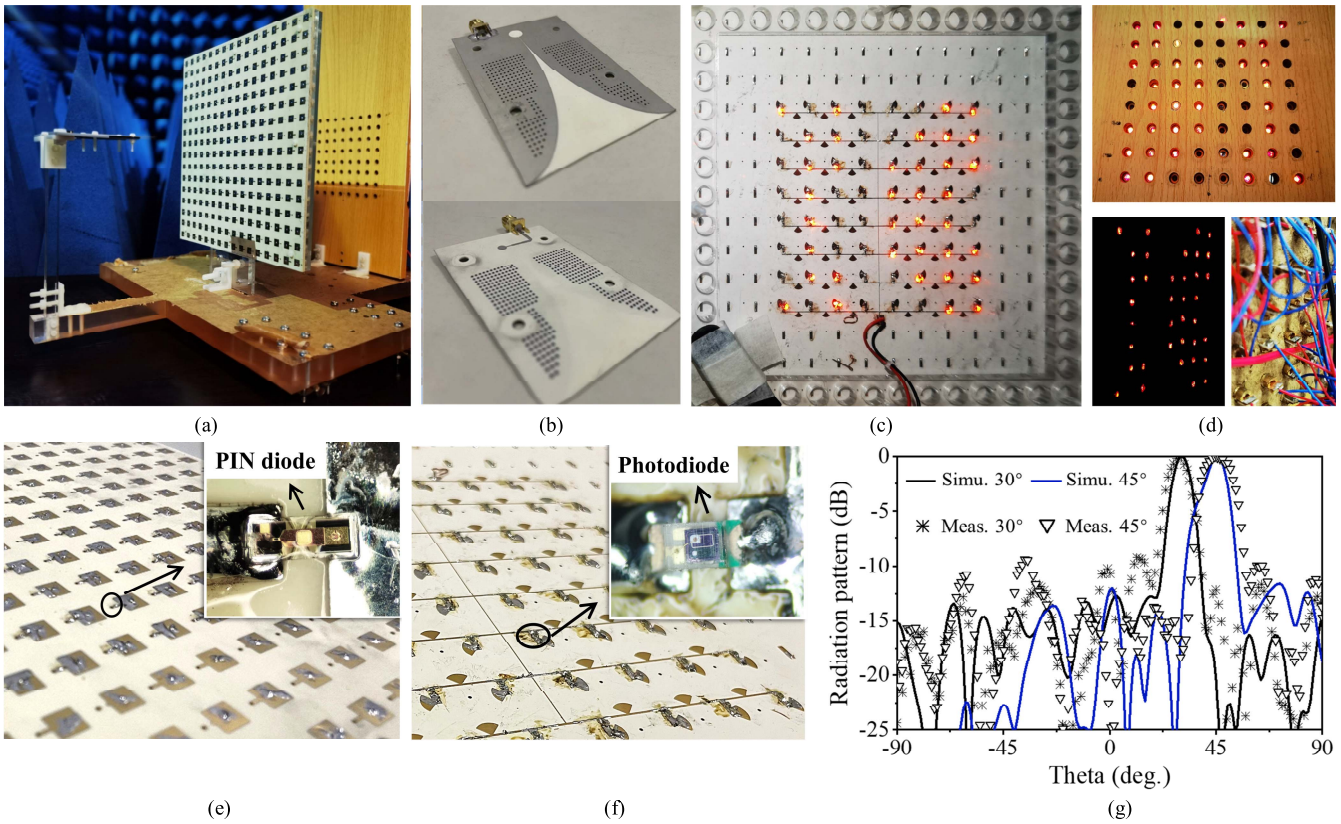

Fig. 14. Experimental validation of the wirelessly reconfigurable RA concept by a scale-reduced 16 × 16 wirelessly reconfigurable RA. (a) Photograph of the fabricated wirelessly reconfigurable RA. (b) Photograph of the fabricated Vivaldi antenna. (c) Illustration of the light-illumination pattern on the PD array on the backside of the array, for a target beam at $\theta = 30°$ and $\varphi = 0°$ (E-plane). (d) Light control system that can be manually reconfigured. During the test in the chamber, ambient light is switched OFF. (e) Top view and (f) bottom view of the fabricated wirelessly reconfigurable RA. (g) Comparison of the simulated and measured radiation patterns in E-plane at 10 GHz for the 16 × 16 wirelessly reconfigurable RA.

to $\theta = 75°$. Therefore, the proposed 1024-element wirelessly reconfigurable RA provides the least scanning range of $\pm 60°$.

Table II lists the comparison of the proposed wirelessly reconfigurable RA with wire-controlled reconfigurable RAs using p-i-n diodes and a single FPGA and a wirelessly controlled reconfigurable metasurface using PCs and varactors. The comparison includes the number of controlling wires, the number of reconfigurable elements, the number of dielectric layers, the tuning mechanisms, and the element spacing. As can be seen, the proposed light-controlled reconfigurable RA achieves the largest scale with the least layers of substrates. It is possible to further increase the number of elements for higher directivity without concerning the wire placement, meaning that the array shall not be limited to the demonstrated 1024 elements.

IV. Experiment and Measurement Results

To validate the concept experimentally, it appears not necessary to build the full 1024-element array since the advantages of the proposed wirelessly reconfigurable RA have been validated in theory and in simulation, where the key tunable components are modeled by measurements. Instead, a smaller-scale wirelessly reconfigurable RA with 16 × 16 elements is designed, fabricated, and measured as a relatively low-cost validation of the proposed concept. The aperture size of the smaller RA is 240 × 240 mm or $8\lambda \times 8\lambda$ at 10 GHz.

Fig. 13 shows the top and bottom views of the 16 × 16 wirelessly reconfigurable RA. To further reduce the validation cost, only an 8 × 8 array of active elements are placed at the center of the RA, surrounded by 192 passive elements. In experiments, the active elements are controlled by light, whereas the passive elements are controlled by manually cutting the traces, as aforementioned. It is argued that the light-control RA can be validated as long as the hybrid-RA achieves a beam steering from one designed angle to the other. In Fig. 13, the active elements are shown in black color and the passive elements in gray. To reconfigure the beam direction, the active elements with p-i-n diodes and the PDs are reconfigured by light, whereas the passive elements are reconfigured manually.

The 256-element wirelessly reconfigurable RA is fabricated and measured in an anechoic chamber built at ShanghaiTech University. Fig. 14(a) shows the photograph of the prototype. Behind the RA is the light control system, where 64 holes are drilled from a wood plate for housing an 8 × 8 array of laser emitters, each for one element. The frame is made of polymathic methacrylate for supporting the Vivaldi antenna, the 16 × 16 wirelessly reconfigurable RA, and the light control system, where $H = 107$ mm for an edge illumination level

of −10 dB. Fig. 14(b) shows the fabricated Vivaldi antenna, where metallic vias are used for the improved mechanical strength of the antenna. Fig. 14(c) shows the light pattern projected on the PD arrays for a targeted beam at $\theta = 30°$ and $\varphi = 0°$, where the associated laser emitters are powered on. Fig. 14(d) shows more details, including the laser emitters inside the holes, the light pattern of higher contrast, and the power supply for the laser emitters. Each laser emitter is manually reconfigured by connecting or disconnecting its power supply. Fig. 14(e) and (f) show the top and bottom views of the proposed wirelessly reconfigurable RA. A battery voltage of $V_{cc} = 6$ V is used to avoid voltage drop during the test. Other values are applicable if V_{cc} is greater than the threshold voltage V_{TH} of the p-i-n diode.

Fig. 14(g) shows the simulated and measured radiation patterns in the E-plane ($\varphi = 0°$) for $\theta = 30°$ and 45°, respectively. As can be seen, the measured main-lobe directions and the 3 dB beamwidths agree well with the simulated results. The measured first sidelobe level is −10 dB, 2 dB worse than that in the simulation. Similar observations are made for other minor lobes. The discrepancies are most likely caused by two factors. First, the fabrication tolerance of the dielectric frame, affects the relative position of the Vivaldi antenna and the reflectarray, leading to slight errors in the phase compensation. Second, the feeding cable of the Vivaldi antenna may block the array radiation. Nevertheless, the slight discrepancy shall not affect the validation of the beam-steering capability of the proposed light-controlled wirelessly reconfigurable RA.

V. Conclusion

The concept of light-controlled large-scale wirelessly reconfigurable microstrip reflectarrays has been proposed and validated by a 1024-element design with a least scanning range of ±60° in simulations and a 256-element design with a light-controlled beam switching capability from 30° to 45° in experiments. With the proposed combination of p-i-n diodes and PDs, the controlling wires are removed from the reflectarray and replaced by light beams, paving the way for developing reconfigurable reflectarrays of multi-polarization, higher gain, and higher frequencies. Beyond reflectarrays, the proposed concept and design of the wirelessly reconfigurable elements may be readily used as basic building blocks for further developing large-scale reconfigurable intelligent surfaces (LRIS) for continuous space coverage, hybrid near-/far-field beamforming, multi-user positioning/sensing, and holographic MIMO system. Also, the proposed concept may enable a new type of microwave-light interface that allows for the embrace of rich and intriguing light-matter interference for further exploration of more advanced meta-devices, such as amplifying metasurfaces, modulating metasurfaces, mixing metasurfaces, computational metasurfaces, and neural-network metasurfaces.

Acknowledgment

The authors would like to thank the support from the NVIDIA Academic Hardware Grant Program. They would like to thank Prof. Qiu Chengwei from the National University of Singapore, Singapore, for useful discussions and comments.

References

[1] B. Di et al., "Hybrid beamforming for reconfigurable intelligent surface based multi-user communications: Achievable rates with limited discrete phase shifts," *IEEE J. Sel. Areas Commun.*, vol. 38, no. 8, pp. 1809–1822, Aug. 2020.

[2] R. Deng, B. Di, H. Zhang, H. V. Poor, and L. Song, "Holographic MIMO for LEO satellite communications aided by reconfigurable holographic surfaces," *IEEE J. Sel. Areas Commun.*, vol. 40, no. 10, pp. 3071–3085, Oct. 2022.

[3] S. V. Hum and J. Perruisseau-Carrier, "Reconfigurable reflectarrays and array lenses for dynamic antenna beam control: A review," *IEEE Trans. Antennas Propag.*, vol. 62, no. 1, pp. 183–198, Jan. 2014.

[4] H. Kamoda, T. Iwasaki, J. Tsumochi, T. Kuki, and O. Hashimoto, "60-GHz electronically reconfigurable large reflectarray using single-bit phase shifters," *IEEE Trans. Antennas Propag.*, vol. 59, no. 7, pp. 2524–2531, Jul. 2011.

[5] E. Carrasco, M. Barba, and J. A. Encinar, "X-band reflectarray antenna with switching-beam using PIN diodes and gathered elements," *IEEE Trans. Antennas Propag.*, vol. 60, no. 12, pp. 5700–5708, Dec. 2012.

[6] J. Han, L. Li, G. Liu, Z. Wu, and Y. Shi, "A wideband 1 bit 12 × 12 reconfigurable beam-scanning reflectarray: Design, fabrication, and measurement," *IEEE Antennas Wireless Propag. Lett.*, vol. 18, no. 6, pp. 1268–1272, Jun. 2019.

[7] Z. Wang et al., "1 bit electronically reconfigurable folded reflectarray antenna based on p-i-n diodes for wide-angle beam-scanning applications," *IEEE Trans. Antennas Propag.*, vol. 68, no. 9, pp. 6806–6810, Sep. 2020.

[8] F. Wu, R. Lu, J. Wang, Z. H. Jiang, W. Hong, and K.-M. Luk, "A circularly polarized 1 bit electronically reconfigurable reflectarray based on electromagnetic element rotation," *IEEE Trans. Antennas Propag.*, vol. 69, no. 9, pp. 5585–5595, Sep. 2021.

[9] S. V. Hum, M. Okoniewski, and R. J. Davies, "Modeling and design of electronically tunable reflectarrays," *IEEE Trans. Antennas Propag.*, vol. 55, no. 8, pp. 2200–2210, Aug. 2007.

[10] F. Venneri, S. Costanzo, and G. D. Massa, "Design and validation of a reconfigurable single varactor-tuned reflectarray," *IEEE Trans. Antennas Propag.*, vol. 61, no. 2, pp. 635–645, Feb. 2013.

[11] E. Baladi, M. Y. Xu, N. Faria, J. Nicholls, and S. V. Hum, "Dual-band circularly polarized fully reconfigurable reflectarray antenna for satellite applications in the Ku-band," *IEEE Trans. Antennas Propag.*, vol. 69, no. 12, pp. 8387–8396, Dec. 2021.

[12] O. Bayraktar, O. A. Civi, and T. Akin, "Beam switching reflectarray monolithically integrated with RF MEMS switches," *IEEE Trans. Antennas Propag.*, vol. 60, no. 2, pp. 854–862, Feb. 2012.

[13] C. Guclu, J. Perruisseau-Carrier, and O. Civi, "Proof of concept of a dual-band circularly-polarized RF MEMS beam-switching reflectarray," *IEEE Trans. Antennas Propag.*, vol. 60, no. 11, pp. 5451–5455, Nov. 2012.

[14] T. Chaloun, F. Tabarani, and S. T. Wipf, "A modular phased array transceiver with RF-MEMS SPDT switches in a 0.25 μm SiGe BiCMOS technology," in *Proc. 12th Eur. Conf. Antennas Propag. (EuCAP)*, 2018, pp. 1–5.

[15] G. Perez-Palomino et al., "Design and experimental validation of liquid crystal-based reconfigurable reflectarray elements with improved bandwidth in F-band," *IEEE Trans. Antennas Propag.*, vol. 61, no. 4, pp. 1704–1713, Apr. 2013.

[16] S. Bildik, S. Dieter, C. Fritzsch, W. Menzel, and R. Jakoby, "Reconfigurable folded reflectarray antenna based upon liquid crystal technology," *IEEE Trans. Antennas Propag.*, vol. 63, no. 1, pp. 122–132, Jan. 2015.

[17] G. Perez-Palomino et al., "Design and demonstration of an electronically scanned reflectarray antenna at 100 GHz using multiresonant cells based on liquid crystals," *IEEE Trans. Antennas Propag.*, vol. 63, no. 8, pp. 3722–3727, Aug. 2015.

[18] X. Li et al., "Broadband electronically scanned reflectarray antenna with liquid crystals," *IEEE IEEE Antennas Wireless Propag. Lett.*, vol. 20, no. 3, pp. 3960–400, Mar. 2021.

[19] W. Yang, C. Zhou, Q. Xue, Q. Wen, and W. Che, "Millimeter-wave frequency-reconfigurable metasurface antenna based on vanadium dioxide films," *IEEE Trans. Antennas Propag.*, vol. 69, no. 8, pp. 4359–4369, Aug. 2021.

[20] K. K. Karnati, M. E. Trampler, and X. Gong, "A monolithically BST-integrated Ka-band beamsteerable reflectarray antenna," *IEEE Trans. Antennas Propag.*, vol. 65, no. 1, pp. 159–166, Jan. 2017.

[21] E. Carrasco and J. Perruisseau-Carrier, "Reflectarray antenna at terahertz using graphene," *IEEE Antennas Wireless Propag. Lett.*, vol. 12, pp. 253–256, 2013.

[22] E. Carrasco, M. Tamagnone, and J. Perruisseau-Carrier, "Tunable graphene reflective cells for THz reflectarrays and generalized law of reflection," *Appl. Phys. Lett.*, vol. 102, no. 10, Mar. 2013, Art. no. 104103.
[23] J. P. Gianvittorio and Y. Rahmat-Samii, "Reconfigurable patch antennas for steerable reflectarray applications," *IEEE Trans. Antennas Propag.*, vol. 54, no. 5, pp. 1388–1392, May 2006.
[24] X. Yang et al., "A broadband high-efficiency reconfigurable reflectarray antenna using mechanically rotational elements," *IEEE Trans. Antennas Propag.*, vol. 65, no. 8, pp. 3959–3966, Aug. 2017.
[25] E. Carrasco, J. Gomez-Cruz, M. Serrano-Berrueco, C. E. Saavedra, and C. Escobedo, "Design of microfluidic reflectarray elements for multi-reconfiguration using liquid metal," *IEEE Open J. Antennas Propag.*, vol. 3, pp. 425–434, 2022.
[26] A. J. Rubio, A.-S. Kaddour, C. Ynchausti, S. Magleby, L. L. Howell, and S. V. Georgakopoulos, "A foldable reflectarray on a hexagonal twist origami structure," *IEEE Open J. Antennas Propag.*, vol. 2, pp. 1108–1119, 2021.
[27] I. V. Shadrivov, P. V. Kapitanova, S. I. Maslovski, and Y. S. Kivshar, "Metamaterials controlled with light," *Phys. Rev. Lett.*, vol. 109, no. 8, Aug. 2012, Art. no. 083902.
[28] X. G. Zhang et al., "Light controllable digital coding metasurfaces," *Adv. Sci.*, vol. 5, no. 11, Aug. 2018, Art. no. 1801028.
[29] X. G. Zhang et al., "An optically driven digital metasurface for programming electromagnetic functions," *Nature Electron.*, vol. 3, no. 3, pp. 165–171, 2020.
[30] R. J. Beneck et al., "Reconfigurable antennas: A review of recent progress and future prospects for next generation," *Prog. Electromagn. Res.*, vol. 171, pp. 89–121, 2021.
[31] S. B. Choi et al., "Nanopattern enabled terahertz all-optical switching on vanadium dioxide thin film," *Appl. Phys. Lett.*, vol. 98, no. 7, Feb. 2011, Art. no. 071105.
[32] H. Yang et al., "A 1600-element dual-frequency electronically reconfigurable reflectarray at X/Ku-band," *IEEE Trans. Antennas Propag.*, vol. 65, no. 6, pp. 3024–3032, Jun. 2017.
[33] X. Pan, F. Yang, S. Xu, and M. Li, "A 10 240-element reconfigurable reflectarray with fast steerable monopulse patterns," *IEEE Trans. Antennas Propag.*, vol. 69, no. 1, pp. 173–181, Jan. 2021.
[34] (2017). *CST Computer Simulation Technology*. [Online]. Available: http://www.cst.com/(CST)
[35] F. Giannini, M. Ruggieri, and J. Vrba, "Shunt-connected microstrip radial stubs (short paper)," *IEEE Trans. Microw. Theory Techn.*, vol. MMT-34, no. 3, pp. 363–366, Mar. 1986.
[36] *MACOM*. Accessed: May 23, 2022. [Online]. Available: https://cdn.macom.com/datasheets/MADP-000907-14020x.pdf
[37] *Shenzhen Chenxinda Technology*. Accessed: May 23, 2022. [Online]. Available: http://www.szxinlei.com/Product/detail/l/cn/id/16.html
[38] S. Y. Miao and F. HanLin, "Boundary-source coherent beamforming using metasurface," in *Proc. IEEE Int. Symp. Antennas Propag. USNC-URSI Radio Sci. Meeting (APS/URSI)*, Dec. 2021, pp. 103–104.
[39] Z. Wang et al., "1 bit electronically reconfigurable folded reflectarray antenna based on p-i-n diodes for wide-angle beam-scanning applications," *IEEE Trans. Antennas Propag.*, vol. 68, no. 9, pp. 6806–6810, Sep. 2020.
[40] H. Yang et al., "A 1-bit 10×10 reconfigurable reflectarray antenna: Design, optimization, and experiment," *IEEE Trans. Antennas Propag.*, vol. 64, no. 6, pp. 2246–2254, Jun. 2016.

Si Yu Miao (Student Member, IEEE) received the B.Eng. degree in electrical engineering from Hunan Normal University, Changsha, China, in 2020. She is currently pursuing the Ph.D. degree in electrical engineering with ShanghaiTech University, Shanghai, China.

Her current research interest includes metasurface antennas and reconfigurable reflectarray.

Feng Han Lin (Senior Member, IEEE) received the B.Eng. and M.Eng. degrees in electrical engineering from Xidian University, Xi'an, China, in 2011 and 2014, respectively, and the Ph.D. degree from the Department of Electrical and Computer Engineering, National University of Singapore (NUS), Singapore, in 2019.

Since 2020, he has been with the School of Information Science and Technology, ShanghaiTech University, Shanghai, China, where he is currently an Assistant Professor. His current research interests include applied electromagnetic theories, metamaterials, antennas, artificial intelligence for electromagnetics, and neural-machine interface.

Dr. Lin was awarded the NUS President's Graduate Fellowship (from 2014 to 2018) and the 2018 Chinese Government Award for Outstanding Self-Funded Students Abroad.